3-dimensional Image Expansion Method by Incorporating RPM Imaging and Full Polarimetric Data for UWB Short Range Radar

Ayumi Yamaryo, Shouhei Kidera and Tetsuo Kirimoto
Graduate School of Informatics and Engineering,
University of Electro-Communications, Japan
Email: kidera@ee.uec.ac.jp

***Abstract*—Ultra wideband (UWB) radar with high range resolution is promising for short-range 3-dimensional (3-D) imaging applications, such as a sensor for rescue robot in disaster scene. We have already proposed the efficient 3-D imaging methods as range point migration (RPM) method, which has a definitive advantage for SAR or time-reversal approaches, in terms of computational burden, high accuracy and high spatial resolution. However, if the aperture size is insufficient, this method cannot image the whole target structure. Conversely, useful information about the target structure can be extracted from the full polarimetric data. Therefore, this paper proposes a novel method that expands reconstructed RPM images by exploiting the full polarimetric data. This method introduces the ellipsoid-based scattering analysis and estimation, and significantly expands the original image by the RPM method by an aggregation of parts of ellipsoids. The results of numerical simulation based on 3-D finite difference time domain (FDTD) analysis verify the effectiveness of our proposed method.**

***Index Terms*—UWB radars, Short range sensing, 3-D sensors, Full polarimetric analysis, Range Points Migration(RPM), Image extrapolation,**

I. Introduction

Ultra wideband (UWB) pulse radar is expected to be adopted in innovative short-range sensing techniques, such as robotic sensors in disaster rescue situations or private watch sensors for independently living elderly or disabled persons. To provide accurate high resolution 3-D images, researchers have investigated various radar imaging methods based on data synthesis, such as synthetic aperture radar(SAR) [1], time-reversal algorithms [2], and range migration methods [3]. However, all of these methods incur impractically large computational burdens, particularly in 3-D imaging problems, and their reconstruction accuracies are insufficient to capture the detailed structures of target shapes. In contrast, the range point migration(RPM) method extracts the 3-D target boundary from range information alone [4], [5], and accomplishes highly accurate 3-D imaging in far less computation time than that required by SAR. The effectiveness of RPM has been widely reported in short-range radar and acoustic imaging studies [6], [7]. However, the image reproduction region obtained by RPM and other conventional methods is, usually limited by the aperture size, and often becomes too narrow to identify the target structure, such as human body or other artificial object.

To alleviate this problem, an image expansion method based on ellipse extrapolation has been proposed [8]. In this method, a target such as human body is approximated by an aggregate of ellipsoids representing the head, trunk and limbs, each clustered RPM image is then extrapolated to a single ellipsoid. Although this method accurately extrapolates ellipsoidal targets even in noisy situations, shapes that significantly differ from ellipsoids (such as tori and cuboids) are naturally degraded by the extrapolation.

To address the above problem, this paper proposes an entirely different approach that utilizes the full polarimetric data for target extrapolation. Full polarimetric data analysis for synthetic aperture radar (SAR), known as polarimetric SAR (PolSAR) analysis, has been extensively reported on [9], [10]. However, in short range situation, such as indoor sensing problem, there are not sufficient studies on polarimetric analysis except for the SAR based approach. Thus, this paper is the first to relate the full polarimetric data in the time domain to the target structure focusing on single ellipsoid. According to this analysis, several significant ellipsoidal parameters can be acquired by a neural network based learning for full polarimetric dataset, at a single antenna location.

Finally, we extrapolated the image from the target points obtained by the RPM method, as an aggregate of ellipsoidal parts (multiple ellipsoids). Utilized on data generated in finite-difference time-domain (FDTD) simulations, the proposed method yielded a significantly more expanded target image than did the original RPM method, even for non-elliptical objects.

II. System Model

Figure 1 shows the system model. An omni-directional antenna is scanned on the x-y plane, where each location is defined as $(X, Y, 0)$. The mono-static radar is assumed. The transmitted signal as current source is defined as mono-cycle pulse with center wavelength λ. It assumes the multiple linear polarizations for the x and y directions in transmitting and receiving, respectively. $s'_{i,j}(X, Y, R')$ denotes the received electric field at the location $(X, Y, 0)$, where $R' = \mathrm{c}t/2$ with t defined as the delay time and c the speed of the radio wave, when the transmitting and receiving polarization are along the $i(x$ or $y)$ axis and $j(x$ or $y)$ axis, respectively. $s_{i,j}(X, Y, R')$

978-1-4673-6555-0/15/$31.00 ©2015 IEEE

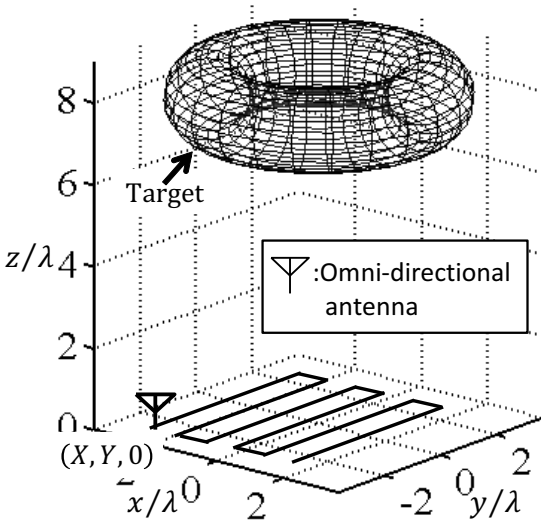

Fig. 1. System model.

is the output of the Wiener filter of $s'_{i,j}(X, Y, R')$. The range point extracted from the local maximum of $s_{x,x}(X, Y, R')$ as to R' is denoted as $\boldsymbol{q} = (X, Y, R)$; the details are given in [4].

III. RPM Method and Extrapolation

We have already established accurate and high-speed 3-D target boundary extraction method as RPM method, which can be applicable to various 3-D target shapes having such as concave surface, edges ridges with 1/100 wavelength accuracy [4], [5]. This method is based on the assumption that a target boundary point (x, y, z) exists on a sphere with its center as the antenna location $(X, Y, 0)$ and its radius as the observed range R. The direction of arrival DOA for each range point $\boldsymbol{q} = (X, Y, R)$, can be determined by assessing the spatial accumulation of intersection points of the spheres, whose center is $(X, Y, 0)$ and radius is R. While this method accomplishes an accurate and fast 3-D imaging, even in richly interfered situation caused by multiple target reflection or noisy environment, it (also SAR or others) suffers from an insufficient imaging region, when the aperture size is small. This insufficiency is an essential problem in radar imaging methods, and should be resolved by other approaches, such as an extrapolation schemes.

As an extrapolation approach, the method [8] has been developed, which is based on ellipse extrapolation of an image obtained by RPM. This method performs ellipse fitting in the data space comprising from range point $\boldsymbol{q}$, which is enabled by the unique feature of RPM imaging [4]. However, this method assumes that the target is shaped similarly to an ellipse and is inaccurate for significantly dissimilar shapes. In addition, multiple targets or complicated target shapes must be correctly clustered; otherwise serious extrapolation error occurs.

IV. Proposed Method

For expanding RPM images to variously shaped targets, this paper proposes a novel method that exploits the full polarimetric data.

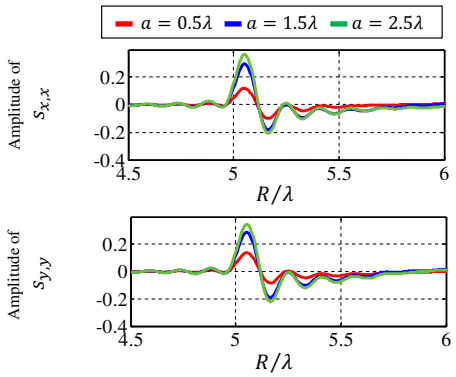

Fig. 2. Outputs of the Wiener filter $s_{x,x}$ and $s_{y,y}$ when $b = 1\lambda$, $c = 0.5\lambda$ and $\theta = 0°$ are fixed.

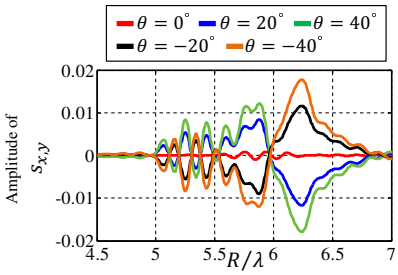

Fig. 3. Outputs of the Wiener filter $s_{x,y}(0, 0, R)$ when θ is variable and other parameters are fixed as $a = 3\lambda$, $b = 2\lambda$ and $c = 0.5\lambda$.

A. Polarimetric analysis for single ellipsoid target

We first investigate the relationship between the time-series waveform of the full polarimetric data and ellipsoid parameters (axial radius and rotation angle). The target is assumed to be a single ellipsoid centered at $(0, 0, z_c)$. The antenna is located at $(0, 0, 0)$. Here, a, b and c are the radii of the ellipsoid along the x-axis, y-axis and z-axis, respectively, and θ is the rotation angle about the z-axis. The observation data are generated by the FDTD method. Figure 2 shows the Wiener filter output of the received signals $s_{x,x}$ and $s_{y,y}$ in the time domain, where the parameter a is varied while other parameters are fixed ($b = 1.0\lambda$, $c = 0.5\lambda$ and $\theta = 0°$). In this figure, the amplitudes of $s_{x,x}$ and $s_{y,y}$ are positively correlated with the axial radius a of the ellipsoid. Figure 3 also shows that of $s_{x,y}$ when θ is varied and the other parameters are fixed as $a = 3.0\lambda$, $b = 2.0\lambda$ and $c = 0.5\lambda$. The received amplitude of $s_{x,y}$ strongly correlates with the rotation angle; moreover, the sign of the phase indicates the rotation direction. Then, the full polarimetric data, especially those of the time-series waveform, contain important information on both the local structure and global expanse of the target shape.

Based on previous analysis, this method first prepares a time-series dataset of various ellipsoids with their a, b, c and θ parameters. The data are preliminarily learned by a neural network as follows. To generate the input data for the time-series waveform, we defined an input vector $\boldsymbol{s}^{\mathrm{nn}}_{i,j}(X, Y, R)(i =$

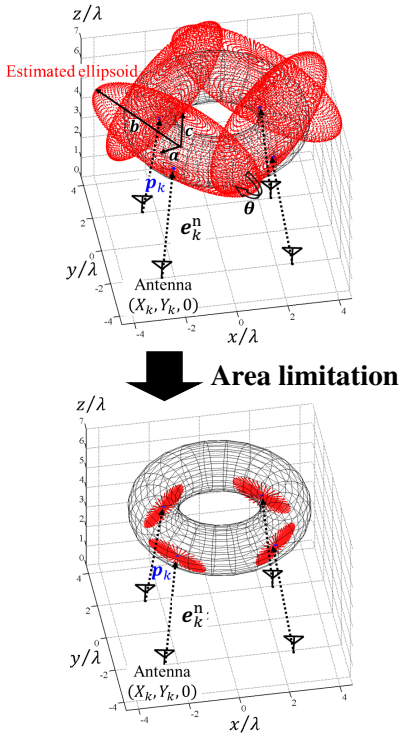

Fig. 4. Example of the extrapolated result by the proposed method.

$x, y, j = x, y)$ for each range point $\boldsymbol{q} = (X, Y, R)$:

$$\boldsymbol{s}_{i,j}^{\mathrm{nn}}(X,Y,R) \equiv [s_{i,j}(X,Y,R), s_{i,j}(X,Y,R+\Delta R), \cdots, s_{i,j}(X,Y,R+(K-1)\Delta R)] \quad (1)$$

where ΔR denotes the sampling interval, and K is a constant natural number. In the training sequence, the input data of the received signal of the antenna located at $(0,0,0)$, namely, $(X,Y) = (0,0)$ are used, for simplicity, where the ellipsoid parameters (a,b,c,θ) are varied.

B. Multiple ellipsoids based extrapolation for RPM image

Our image extrapolation methodology fits each RPM target point to an ellipsoid with parameters estimated by the above neural network approach. In the literature [8], each group of target points obtained by RPM was extrapolated as a single ellipsoid, which is problematic for shapes that widely differ from ellipsoids. Thus, the proposed method expresses each target point obtained by RPM as part of an ellipsoid; that is, a single target shape is expressed as an aggregation of partial ellipsoids. In this sense, our method differs from that of [8]. Figure 4 illustrates the basic concept of the multiple ellipsoid-based extrapolation scheme.

Here, the boundary point on the ellipsoid with the estimated parameters $(\hat{a}, \hat{b}, \hat{c}, \hat{\theta})$ for each range point $\boldsymbol{q}_k$is expressed as

$$\begin{pmatrix} x_k^E \\ y_k^E \\ z_k^E \end{pmatrix} = \boldsymbol{R}_z(\hat{\theta}) \begin{pmatrix} \hat{a}\cos\phi\cos\psi \\ \hat{b}\cos\phi\sin\psi \\ \hat{c}\sin\psi \end{pmatrix} + \begin{pmatrix} 0 \\ 0 \\ Z_k - \hat{z}_c \end{pmatrix} \quad (2)$$

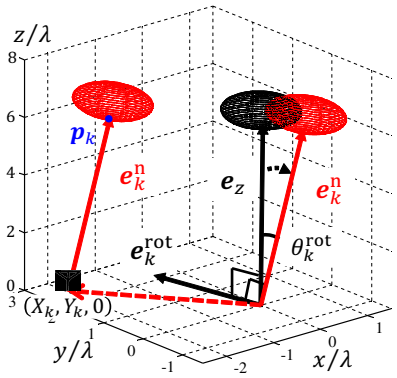

Fig. 5. Ellipsoid rotation and translation along the LOS direction $\boldsymbol{e}_k^{\mathrm{n}}$.

where $Z_k = R_k + \hat{c}/2$, $\boldsymbol{R}_z(*)$ denotes the rotation matrix along the z axis, ϕ and ψ are azimuthal and elevation angles of the ellipsoid, respectively. Applying RPM to the range points $\boldsymbol{q}_k = (X_k, Y_k, R_k)$, we also estimated a corresponding target point $\boldsymbol{p}_k = (x_k, y_k, z_k)$. Note that each target point $\boldsymbol{p}_k$ satisfies a one-to-one correspondence with each range point $\boldsymbol{q}_k$; this feature is unique to RPM imaging. Under the assumption that the antenna receives a strong echo from the target boundary, which is perpendicular to the line of sight (LOS) direction on $\boldsymbol{p}_k$, the unit vector of the LOS direction, that is, normal vector on target boundary, is calculated as $\boldsymbol{e}_{\mathrm{n},k} = (\boldsymbol{p}_k - (X_k, Y_k, 0))/||\boldsymbol{p}_k - (X_k, Y_k, 0)||$. In addition, since the target boundary should be tangent to the plane orthogonal to this normal vector, the extrapolating ellipse should also be tangent to the target boundary. For simplicity, we assume that the tangential point of each ellipsoid is located, at an elevation angle $\psi = -\pi/2$.

Then, the LOS direction in the learning process, namely, $\boldsymbol{e}_z = (0,0,1)$, is converted to that for each range point $\boldsymbol{q}_k$ according to $\boldsymbol{e}_k^{\mathrm{n}}$. According to this conversion, each point (x_k^E, y_k^E, z_k^E) on estimated ellipsoid boundary is converted as;

$$(\tilde{x}_k^E, \tilde{y}_k^E, \tilde{z}_k^E)^{\mathrm{T}} = \boldsymbol{R}_k(\boldsymbol{e}_k^{\mathrm{rot}}, \xi_k^{\mathrm{rot}})(x_k^E, y_k^E, z_k^E)^{\mathrm{T}} + (X_k, Y_k, 0)^{\mathrm{T}}, \quad (3)$$

where the matrix $\boldsymbol{R}_k(\boldsymbol{e}_k^{\mathrm{rot}}, \xi_k^{\mathrm{rot}})$ denotes 3-dimensional rotation along the axis $\boldsymbol{e}_k^{\mathrm{rot}} = \dfrac{\boldsymbol{e}_z \times \boldsymbol{e}_k^{\mathrm{n}}}{|\boldsymbol{e}_z \times \boldsymbol{e}_k^{\mathrm{n}}|}$ with the angle $\xi_k^{\mathrm{rot}} = \cos^{-1}(\boldsymbol{e}_z \cdot \boldsymbol{e}_k^{\mathrm{n}})$.

Finally, a part of ellipsoid is extracted as $\hat{\Omega}_k$ is extracted for each $\boldsymbol{q}_k$, where the ranges of azimuth and elevation angles are limited as $0 \le \phi \le 2\pi, -\pi/2 \le \psi \le \psi_{\mathrm{E}}$ in , where ψ_E is determined empirically. Then, the extrapolated image $\hat{\Omega}_{\mathrm{ex}}$ is determined as $\hat{\Omega}_{\mathrm{ex}} = \bigcup_k \hat{\Omega}_k$. The lower side of Fig. 4 denotes the area limitation example, described above.

V. Performance Evaluation in Numerical Simulation

This section describes the two types of performance evaluations. One is the evaluation for neural network based learning

TABLE I
ESTIMATION RESULTS FOR THE NEURAL NETWORK BASED PARAMETER ESTIMATION OF SINGLE ELLIPSOID.

True (a/λ,b/λ,c/λ,θ/deg)	Estimated (a/λ,b/λ,c/λ,θ/deg)	Relative error (a,b,c,θ)[%]
(1.70,1.00,2.50,30.0)	(1.72,0.97,2.51,28.0)	(1.14,2.68,0.28,6.76)
(1.50,2.20,3.00,20.0)	(1.51,2.18,3.00,21.7)	(0.85,0.73,0.05,8.53)
(1.00,2.00,2.70,40.0)	(1.01,2.01,2.69,43.2)	(0.62,0.56,0.24,7.99)
(2.00,1.50,1.00,-35.0)	(2.02,1.48,0.97,-37.0)	(0.97,1.48,3.48,5.39)
(1.40,2.80,2.00,10.0)	(1.40,2.82,2.01,9.6)	(0.33,0.64,0.36,3.68)
(1.00,2.00,2.40,-15.0)	(1.02,2.01,2.39,-14.9)	(1.76,0.67,0.22,0.55)
(2.80,1.70,1.10,35.0)	(2.81,1.74,1.16,36.6)	(0.35,2.46,5.00,4.57)

using full polarimetric data, where unknown parameters of ellipsoid are estimated by the neural network with time-series data base. The other demonstrates the performance of image extrapolation by our proposed method, namely, multiple ellipsoid based extrapolation for RPM imaging points.

A. Ellipsoid parameter estimation by neural network

This section reports on the parameter estimation of a single ellipsoid from the full polarimetric dataset. The antenna is located at $(x, y, z) = (0, 0, 0)$. During the learning stage of the neural network, the parameters a, b and c of the training ellipsoids are varied as $0.5\lambda, 1\lambda, 1.5\lambda, 2\lambda, 2.5\lambda$ and 3λ, and θ is varied as $-40°, -30°, -20°, -10°, 0°, 10°, 20°, 30°$ and $40°$, respectively. All of these a, b, c and θ combinations are used as the training data. The conductivity and relative permittivity of the ellipsoid target are set to $1.0 \times 10^7 \mathrm{S/m}$ and $\epsilon = 1.0$, respectively. The observation data are generated by the FDTD method assuming a noiseless situation. The neural network contains three hidden layers, with 30 neurons in the first layer, 20 in the second layer, and 10 in the final layer. Here, $K\Delta R = 1.44\lambda$, and the sample interval of range as $\Delta R = 0.03\lambda$ are set in Eq. (1). Table I lists the parameters of the ellipsoid targets estimated by the trained neural network. The untrained parameters are depicted in red font. From this table, it can be observed that the time-series based neural network accurately estimated the ellipsoidal parameters. The average relative errors in a, b, c and θ are 2.7%, 2.3%, 1.3% and 6.9%, respectively.

B. Extrapolation Performance

This subsection presents the extrapolation results of our proposed method. The transmitting and receiving antenna set is scanned over the area $-2.5\lambda \le x, y \le 2.5\lambda$ at 0.5λ intervals in the x and y directions. Again, the observation data are generated by the FDTD method. In RPM imaging, the set of range points $\boldsymbol{q}_{x,x}$ extracted by $s_{x,x}(X, Y, R')$ is used only in the initial 3-D imaging. Figures 6 and 7 show the target points obtained by RPM and the extrapolation expression of the proposed method, respectively. The target is the torus shown in Fig. 1. Here, the elevation angle of each ellipsoid is limited to $(\psi_E = -4\pi/9 : -\pi/2 \le \psi \le -4\pi/9)$. According to these figures, the proposed method significantly enhances the imaging region of the torus boundary, which is dissimilar to an ellipsoid. However, there are non-negligible

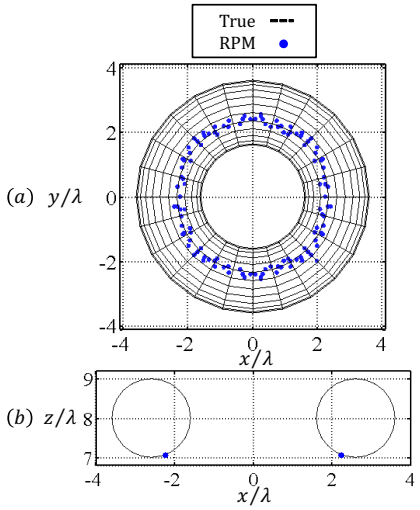

Fig. 6. Target boundary points by RPM method (a: projection to x-y plane, b: cross-section for y=0 plane.).

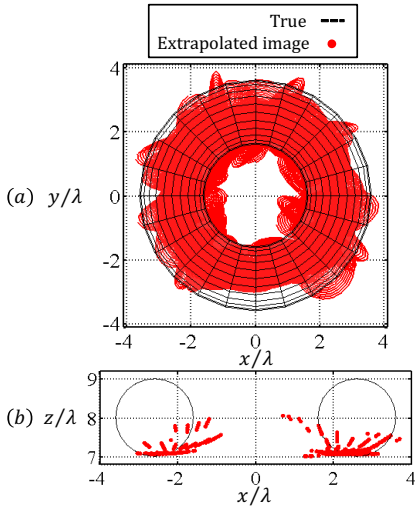

Fig. 7. Extrapolated image of the proposed method (a: projection to x-y plane, b: cross-section for y=0 plane.).

extrapolation errors. These errors result from the inaccurate estimation of the ellipsoid parameters from time-series data, because each antenna receives multiple reflection echoes from the torus boundary. To prevent this interference effect, the windowing time span for extracting the time series data should be appropriately determined.

Here, the image extrapolation is quantitatively analyzed by investigating the effective reconstruction image region, namely, the extrapolation effect. For this evaluation, first, a whole true target boundary denoted as $\Omega_{\mathrm{all}}^{\mathrm{true}}$ is divided into small regions with the same area as $\Delta\Omega_i^{\mathrm{true}}, (i = 1, 2, \cdots, N_{\mathrm{tar}})$. A whole target boundary region is expressed as $\Omega_{\mathrm{all}}^{\mathrm{true}} = \bigcup_i \Delta\Omega_i^{\mathrm{true}}$. Also, the center point for the region $\Delta\Omega_i^{\mathrm{true}}$ is defined as $\boldsymbol{p}_i^{\mathrm{true}}$. Then, for the k-th estimated target point denoted as $\boldsymbol{p}_k^{\mathrm{est}}$, the estimated effective image area $\hat{\Omega}_k^{\mathrm{eff}}$

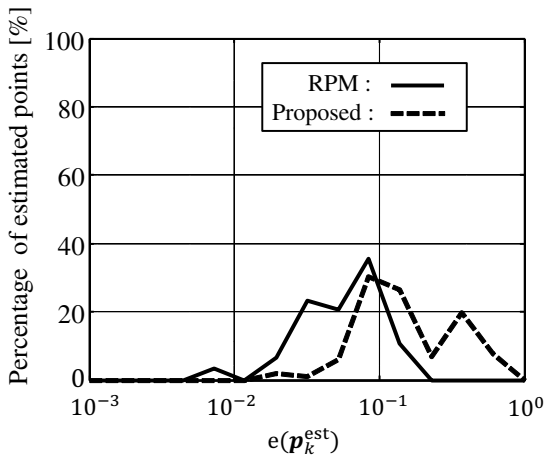

Fig. 8. Number of the estimated target points.

is defined as;

$$\hat{\Omega}_k^{\mathrm{eff}} = \left\{ \bigcup_i \Delta\Omega_i^{\mathrm{true}} \;\middle|\; \|\boldsymbol{p}_i^{\mathrm{true}} - \boldsymbol{p}_k^{\mathrm{est}}\| \le \delta_p \right\}, \tag{4}$$

where δ_p is threshold for extracting effective image region. $\delta_p = 0.1\lambda$ is used in this case. The effective image area $\hat{\Omega}^{\mathrm{eff}}$ composed of all target points is defined as; $\hat{\Omega}^{\mathrm{eff}} = \bigcup_k \hat{\Omega}_k^{\mathrm{eff}}$. As the evaluation value for image extrapolation effect, the reconstruction ratio is defined as; $P_{\mathrm{a}} = S_{\mathrm{eff}}/S_{\mathrm{true}}$, where S_{true} and S_{eff} denote the areas of $\Omega_{\mathrm{all}}^{\mathrm{true}}$ and $\hat{\Omega}^{\mathrm{eff}}$, respectively. The percentage reconstruction ratio P_{a} is 3.0 % in RPM method and 29.3 % in the proposed method, respectively. Clearly, the proposed method significantly expands the target image, even when the target deviated from an ellipsoid.

However, there are non-negligible errors in extrapolation as shown in Fig. 7. Although it significantly enhances the reconstruction ratio, extrapolation accuracy requires an additional evaluation criterion. The error in the image reconstruction is given by

$$\mathrm{e}(\boldsymbol{p}_k^{\mathrm{est}}) \equiv \min_{\boldsymbol{p}_{\mathrm{true}}} \left\| \boldsymbol{p}_k^{\mathrm{est}} - \boldsymbol{p}^{\mathrm{true}} \right\| \quad (k = 1, 2, \ldots, N_{\mathrm{est}}), \tag{5}$$

where $\boldsymbol{p}^{\mathrm{true}}$ denotes the true target points with sufficiently dense sample and N_{est} denotes the total number of the estimated points. Figure 8 plots the number of estimated points with error $\mathrm{e}(\boldsymbol{p}_k^{\mathrm{est}})$ in extrapolations of ellipsoidal and toroidal targets, respectively. While the proposed method and RPM yield the same reconstruction accuracy of ellipsoidal targets, RPM better reconstructs the toroidal target, because of the aforementioned interference effect in the proposed method. However, the maximum error in the toroidal target is within 1 λ, and the apparent extrapolated image does not markedly deviate from the actual target shape. The percentages of estimated target points satisfying $\mathrm{e}(\boldsymbol{p}_k^{\mathrm{est}}) \le 0.1\lambda$ are 89.3 % for the RPM method and 58.3 % for the proposed method, respectively, which helps us to recognize the shape of the target, especially for target size. Clearly, the percentage of accurately estimated target points (extrapolated points) is reduced when our method is applied to toroidal objects. This inaccuracy must be addressed in our future work.

VI. Conclusion

This paper proposed a novel 3-D image extrapolation method that incorporates the RPM method but exploits the full polarimetric dataset. In a time-series data analysis of full polarimetric data, the co-polarization and cross-polarization data were strongly correlated with the radius and rotation angle of a single ellipsoid. By neural-network learning of the ellipsoid parameters, the target was accurately estimated from the time-series data only received by a single antenna. Next, to expand the reproduced image, we combined the RPM method with single ellipsoid estimation by the full polarimetric data. In fitting ellipsoids to the RPM target points, we exploited the one-to-one correspondence between the target and the range points. Finally, in FDTD simulations, we verified that the reconstruction ratio is much higher in the proposed method than in the original RPM method, even for decidedly non-ellipsoidal target shapes.

Acknowledgment

This work is supported in part by the Grant-in-Aid for Young Scientists (B) (Grant No. 23760364), promoted by JSPS, the Research Grant promoted by KDDI funcation.

References

[1] D. L. Mensa, G. Heidbreder and G. Wade, "Aperture Synthesis by Object Rotation in Coherent Imaging," *IEEE Trans.NuclearScience Sensing*., vol.27, no.2, pp.989-998, Apr. 1980.

[2] A. J. Devaney, "Time Reversal Imaging of Obscured Targets From Multistatic Data", *IEEE Trans.Antennas Propag*., vol.53, no.5, pp.1660-1610, May, 2005.

[3] F. Soldovieri, A. Brancaccio, G. Prisco, G. Leone, and R. Pieri, "A Kirchhoff-based shape reconstruction algorithm for the multimonostatic configuration: The realistic case of buried pipes", *IEEE Trans.Geosci. RemoteSens*., vol.46, no.10, pp.3031-3038, Oct, 2008.

[4] S. Kidera, T. Sakamoto, and T. Sato, "Accurate UWB Radar 3-D Imaging Algorithm for Complex Boundary without Range Points Connections," *IEEE Trans. Geosci. & Remote Sens.*, vol.48, no. 4, pp. 1993–2004, Apr., 2010.

[5] S. Kidera, T. Kirimoto, "Efficient 3-dimensional Imaging Method Based on Enhanced Range Points Migration for UWB Radars," *IEEE Geosci. & Remote Sens. Letters*, vol.10, no. 5, pp. 1104–1108, Sep., 2013.

[6] R. Salman, I. Willms, "3D UWB Radar Super-Resolution Imaging for complex Objects with discontinous Wavefronts," 2011 IEEE International Conference on Ultra-Wideband (ICUWB), Sep. 2011.

[7] H. Taki, S. Tanimura, T. Sakamoto, T. Shiina and T. Sato, "Accurate ultrasound imaging based on range point migration method for the depiction of fetal surface," Journal of Medical Ultrasonics, September 2014.

[8] Y. Abe, S. Kidera and T. Kirimoto, "Accurate Image Expansion Method Using Range Points Based Ellipse Fitting for UWB Imaging Radar," *IEICE Trans. & Commun.*, vol. E95-B, no. 7, pp. 2424-2432, July., 2012.

[9] Y. Yamaguchi, T. Moriyama, M. Ishido, and H. Yamada., "Four-Component Scattering Model for Polarimetric SAR Image Decomposition," *IEEE Trans. Geosci. Remote & Sens.*, vol.43, no. 8, pp. 1699–1706, Apr., 2005.

[10] S. Sauer, T. Jaghuber, F. Kugler, "Orientation angle estimation over forested terrain using P-band POLSAR data," *IEEE Trans. Geosci. Remote & Sens.*, pp. 5137-5140, July., 2012.